Received: 15 March 2024 | Revised: 30 May 2024 | Accepted: 26 June 2024

DOI: 10.1002/rra.4347

RESEARCH ARTICLE

WILEY

Anchor chains—A simple low-cost device to assist passage of small-bodied mass fish

Jason Harley | Hui Ling Wong | Hubert Chanson

School of Civil Engineering, The University of Queensland, Brisbane, Queensland, Australia

Correspondence
Jason Harley, School of Civil Engineering, The University of Queensland, Brisbane QLD 4072, Australia.
Email: j.harley@uq.net.au

Abstract

Attention has been placed on a variety of barriers that hinder fish passage in modern times. The most prevalent fish barriers were culverts which have negatively impacted waterway connectivity and fish habitats. For small-bodied mass fish, high barrel velocities and turbulence have reduced fish swimming performance because of their weak swimming capabilities. In the present study, physical testing was conducted under controlled flow conditions to assess the extent and magnitude of turbulence characteristics, secondary flow and low-velocity zones in a 0.5-m-wide box culvert barrel. Two cases were investigated; a reference case consisting of a smooth rectangular channel and a low-cost design solution to improve upstream fish migration consisting of a single galvanized anchor chain fitted within a smooth rectangular channel. The single anchor chain was positioned towards one corner of the channel to induce asymmetric flow, reducing overall energy losses and enhancing the existing low-velocity zone in the adjacent channel corner. The anchor chain induced a strong turbulent flow motion away from the anchor chain, characterized by higher Reynolds stress and turbulent kinetic energy, along with a distinct channel flow asymmetry. Conversely, the low-velocity zone, between the anchor chain and the bottom channel corner, was significantly expanded with reduced longitudinal mean velocities and turbulent scales. Whilst the anchor chain link contributed to some complex localized wake flow, the anchor chain also influenced the distributions of normal turbulent stresses ($v'_z{}^2 - v'_y{}^2$), which in turn influenced the location of secondary flow cells. This secondary flow redirected low momentum fluid into the low-velocity zones, setting the conditions for the favorable upstream passage of small-bodied mass fish species.

KEYWORDS

anchor chain, box culverts, developing countries, fish passage, friction factors, low-velocity zones, physical modelling, secondary flow

1 | INTRODUCTION

1.1 | Culverts as barriers

The protection and enhancement of fish passage is a valuable economic, conservation, and socio-cultural focus for advanced and developing societies (Lynch et al., 2016). Modern attention has focused on a variety of barriers to fish passage, and these include dams, weirs, culverts, and other forms of river regulation (Rolls et al., 2013). These barriers range from vertical drops, inadequate light, adverse thermal and water chemistry levels, excessive velocities, and turbulence levels (Jones & Hale, 2020; Silva et al., 2018). The most prevalent fish barriers were culverts, which were an indispensable requirement for modern transportation networks (Goerig et al., 2016), and typically take the form of box culverts or circular pipe culverts. These culverts typically comprise an inlet and outlet structure linked by a conduit (barrel). Examples of box culverts and circular pipe culverts with baffles fitted to the culvert barrel to assist fish passage are shown in Figure 1. Whilst bridges were typically recommended by fish management agencies for cross-drainage fish passage solutions, their higher capital cost precluded their use for low-discharge applications (Jones & Hale, 2020). The economic design of culverts typically focused on maximizing discharge capacity whilst minimizing cross-sectional area for the benefit of lower construction materials cost (Chanson & Leng, 2019). This traditional engineering strategy mainly resulted in culverts exhibiting high barrel velocities and homogenous velocity fields which were detrimental to fish and other aquatic species.

1.2 | Impact on small-bodied fish

Fish passage studies have predominantly focused on Northern hemisphere environs involving species of economic significance such as salmonids. In comparison, little studies have been completed in the Southern hemisphere, where the outcomes of salmonid studies were not ideally suited to the management of endemic juvenile and small-bodied mass fish (Birnie-Gauvin et al., 2019; Miles et al., 2013; Stuart & Mallen-Cooper, 1999). Australian freshwater fish are mostly endemic, either diadromous or potamodromous, and migrate within a range of riverine environments, including ephemeral streams (Humphries & Walker, 2013; Pusey et al., 2004). Many of these are juvenile and small-bodied mass fish and tend to display weak swimming performance when migrating upstream (Hurst et al., 2007; Rodgers et al., 2014; Tudorache et al., 2008). Swimming performance varies significantly in natural populations depending on species, body length, and the hydraulic conditions arising from specific barriers (Jones & Hale, 2020). Swimming performance is typically assessed against U_{crit} data, which is assumed to estimate the maximum sustained swimming speed (Beamish, 1978), and U_{sprint} data, which is assumed to estimate the burst speed of fish (Starrs et al., 2011). For endemic small-bodied and juvenile fish, U_{crit} values typically ranged from 0.1 to 0.6 m/s (Humphries & Walker, 2013; Hurst et al., 2007), whilst U_{sprint} data ranged from 0.4 to 0.9 m/s (Starrs et al., 2011). For road culverts between 12 and 30-m length, these values could result in fish taking longer to navigate culverts which could lead to fatigue. Culverts can transport large-scale energetic turbulence from upstream sources which can destabilize and disorientate small-bodied fish. While many studies indicate that fish swimming performance decrease with increased turbulence (Enders et al., 2003; Pavlov et al., 2000), other studies indicate that swimming performance may be improved in zones of high velocity and zones of decreased turbulence (Smith et al., 2005). This variation may be due to some fish species harnessing aspects of turbulence during swimming (Liao, 2007). However, it is realistic to assert that turbulence metrics cannot explain all observed swimming behaviors in fish (Goettel et al., 2015). Despite this, investigating the range of turbulent flow properties that interact with the swimming behaviors of small-bodied fish species remains important. (Chanson & Leng, 2021; Lacey et al., 2012).

FIGURE 1 Box culverts in Australian fish mapped waterways (Ensilon Consulting, 2024). (LEFT) 3.0 m × 3.0 m reinforced concrete box culvert (RCBC) cell fitted with full-height vertical wall fish baffles at Flagstone, Queensland, Australia. (RIGHT) "Quad" fish baffles fitted to a 1.05-m-diameter reinforced concrete pipe (RCP) at Walloon, Queensland, Australia. For further details on "Quad" fish baffles refer to Kapitzke (2010). [Color figure can be viewed at wileyonlinelibrary.com]

1.3 | Problems with fish passage devices

A variety of measures were previously devised to improve the likelihood of fish passage in new and retrofitted box culverts. Invert baffles were the traditional means for improving fish passage with the first recorded laboratory trials in the 1950s (Shoemaker, 1956). Baffle configurations were subsequently refined and adapted configurations included invert mounted offset baffles (Rajaratnam et al., 1988) and similar invert mounted devices such as slotted weirs, weir baffles, and spoiler baffles (Rajaratnam et al., 1989; Rajaratnam et al., 1991; Rajaratnam & Katopodis, 1990). These baffles worked on the principle of "plunging flow" during low-submergence low-discharge conditions and "streaming" (or "skimming") flow for higher discharges (Katopodis, 1992). Localized low-velocity zones (LVZ) and resting points existed between the baffles. However, due to a lack of a contiguous longitudinal LVZ, fish passage success rates were highly dependent on longitudinal baffles spacings, where larger baffle spacings resulted in poor fish passage performance (Katopodis, 1992; Rajaratnam & Katopodis, 1990). Depending on the culvert aspect and aperture size, baffles adversely impacted the overall discharge capacity of the culvert barrel (Chanson & Leng, 2021; Larinier, 2002). To address this, alternative configurations were implemented to reduce discharge impacts, and examples of these included longitudinal beams (Sanchez et al., 2020), small triangular corner baffles (Cabonce et al., 2018; Cabonce et al., 2019), and mussel spat ropes (David et al., 2009; David et al., 2014; Kozarek & Hernick, 2018; Tonkin et al., 2012). However, many contemporary installations still relied on variants of earlier large baffle designs that resulted in sizable wake and recirculation zones between baffles. This was evident in the jurisdictional case of Queensland Australia, where the "deemed to comply" box culvert solution comprised full-height wall-mounted baffles (DAF, 2018). These full-height wall-mounted baffles were the subject of limited laboratory trials (Leng & Chanson, 2020) and field investigations (Marsden, 2015). In the case of an investigation by Li and Chanson (2020), full-height side-mounted baffles resulted in significant reduction in discharge as well as seiching fluid motion that could potentially disorientate fish.

1.4 | The anchor chain

New and retrofit installations of full-height side-mounted baffles represented a considerable proportion of overall materials, fabrication, and construction cost budgets for culverts (Ensilon Consulting, 2024). Furthermore, large baffle sets may reduce discharge capacity, increase blockage risk, increase upstream flood levels, and increase safety risks during major storm events (Ball et al., 2019). Consequently, simple low-cost low-impact fish passage solutions for box culverts are needed. The inspiration for this novel solution combined three recent research insights. Firstly, the findings from hydrodynamic tests on mussel spat ropes adapted to fish passage (Kozarek & Hernick, 2018). Whilst mussel spat ropes were originally aimed to assist climbing fish such as *kokopu Galaxias fasciatus*, mussel spat ropes installed in culverts created hydraulic conditions that enhanced the swimming capability of small-bodied mass fish (David et al., 2009; Kozarek & Hernick, 2018). Based on physical modelling and field testing of mussel spat ropes in box culverts, mussel spat ropes provided a small LVZ surrounding the rope circumference suitable for small-bodied fish, with a minimal reduction in culvert barrel discharge. Secondly, insights into the phenomena of LVZs in the bottom corner of box culverts, which were comprehensively documented by previous researchers (Cabonce et al., 2018; Chanson & Leng, 2021; Wang & Chanson, 2018; Zhang & Chanson, 2018). Based on early research on square conduits (Gerard, 1978; Gessner, 1973), the occurrence of LVZs in box culvert corners were associated with secondary flow. This was also associated with turbulent shear stress gradients originating from abrupt channel variations such as roughness or sharp corners (Tominaga et al., 1989). Thirdly, the application of hydrodynamic asymmetry to the design of fish passage devices. This approach was adopted by Li et al. (2022), where a 60 × 20 mm longitudinal rail with sharp edges was asymmetrically installed, at 30 degrees to the vertical, in a semi-circular section to induce asymmetrical flow. In this example, the presence of distinct secondary flow cells was evident. It was also noted that two modest sized LVZs adjacent to the longitudinal rail were present, whilst discharge capacity impacts were minor. Similarly, Wang and Chanson (2018) installed sidewall roughening on one side of a rectangular channel, which resulted in the enlargement of the bottom corner LVZ and further lowered localized streamwise velocities.

In this paper, we investigate the use of anchor chains to further enhance LVZs in the bottom corners of box culverts. Anchor chains were chosen as it may offer an alternative to mussel spat ropes and address some of the operational issues reported by Kozarek and Hernick (2018) such as rope failure, loss of fiber mass, and potential microplastic pollution to the environment. The experiments were conducted in a hydraulic flume under controlled conditions to replicate open channel flow in a smooth box culvert. Three modelling cases were investigated: a reference case which consisted of a smooth rectangular channel; and two design cases which incorporated a single 8 and 13 mm diameter anchor chain, asymmetrically set on the channel invert adjacent to the right wall.

2 | PHYSICAL FACILITIES AND EXPERIMENTAL TESTING

2.1 | Experimental facility and instrumentation

Experimental testing was conducted in the AEB Hydraulics Laboratory at the University of Queensland using a 15 -m-long 0.5-m-wide horizontal rectangular flume, ending with a free-edge overfall. The slope was set at 0% to allow comparison with other culvert testing programs (Chanson, 2020; Leng & Chanson, 2020; Li et al., 2022; Wang & Chanson, 2018) as well as to reflect on field observations with most box culverts constructed with little fall and in some instances set flat (DAF, 2018). The water discharge was measured by

an in-line Venturi meter installed and calibrated in accordance with British Standards (1943). Rail-mounted pointer gauges were used to measure flow depths. For cross-sectional velocity measurements, boundary velocities were measured at approximately 20 mm spacing using the Prandtl Pitot tube, whilst 15 vertical profiles were measured using both Prandtl Pitot tube Dwyer™ 166 Series (diameter = 2.98 mm) and the acoustic Doppler velocimeter (ADV) Nortek™ Vectrino+ fitted a side-looking probe. A minimum of 14 measurements were conducted per vertical profile. For locations adjacent to the anchor chain and sidewall, where instrument access was difficult, velocity measurements were supplemented using the roving Preston tube C1.6R variant (diameter = 1.43 mm), and the acoustic Doppler velocimeter Nortek™ Vectrino II (Profiler) fitted with a down-looking probe set at an angle of 30° to the vertical axis. The roving Preston tube C1.6R variant was calibrated to the Prandtl Pitot tube results obtained at $y = 0.250$ m (Sanchez et al., 2018). The vertical location of all instruments was recorded with a HAFCO® digital scale unit with an accuracy of 0.05 mm for the 13 and 8 mm anchor chain case. The ADV Vectrino+ was sampled at 200 Hz for each measurement point; for the smooth rectangular channel, 36,000 samples were taken, whilst 50,000 samples were taken for the smooth rectangular channel fitted with the single 13 mm diameter anchor chain. The ADV Profiler was sampled at 100 Hz for 50,000 samples. The ADV data were processed by removing erroneous data with an average signal-to-noise ratio (SNR) of less than 5 dB and an average correlation value (across all beams) of less than 60%. Statistical outliers were then removed using the phase-space thresholding (PST) technique and followed by data replaced using linear interpolation (Goring & Nikora, 2002; Wahl, 2003). The ADV was unable to measure velocities at the free surface; however, these were estimated using the last vertical reading in the profile. Dye injections were employed to visualize flow motion, complemented by digital photography and video recordings.

2.2 | Anchor chain treatment

The 0.5-m-wide horizontal rectangular flume was fitted with a single galvanized anchor chain. The dimensions of the anchor chain were generally in accordance with Table 2 of Australian Standards (2004)

TABLE 1 Galvanized anchor chain and installation dimensions.

Diameter of anchor chain	Link length (mm)	Link width (mm)	Overall installed chain width (mm)	Overall installed chain depth (mm)	Installed offset from right wall (mm)
8 mm	48	30	26	21	42
13 mm	77	47	42	42	39

TABLE 2 Comparison of results between smooth rectangular channel and smooth rectangular channel fitted with a single anchor chain, longitudinal location at $x = 8.0$ m, channel width (B) = 0.5 m, bed slope (S_o) = 0%, discharge (Q) = 0.0556 m^3/s.

	V_x(mean) (m/s)	V_x(max) (m/s)	Bulk Reynolds number (Re)	Froude number (Fr)	Depth (d) (m)	Darcy-Weisbach friction factor (f)
Smooth rectangular channel	0.79	0.86	340,900	0.68	0.140	0.019
Smooth rectangular channel fitted with an 8 mm diameter chain	0.77	Did Not Record	335,600	0.65	0.145	0.025
Smooth rectangular channel fitted with a 13 mm diameter chain	0.75	0.88	343,400	0.62	0.147	0.031

FIGURE 2 13 mm diameter galvanized anchor chain. (LEFT) single anchor chain set in the smooth rectangular channel with an offset of 39 mm from the side wall (photograph taken at $x = 12$ m, facing upstream). (RIGHT) 13 mm diameter anchor chain link dimensions. [Color figure can be viewed at wileyonlinelibrary.com]

AS 4177.4-2004. The anchor chain dimensions are highlighted in Table 1.

The near edge of the anchor chain was set close to the right-hand flume wall to induce flow asymmetry in the channel cross-section and enhance the bottom right-hand corner LVZ (Figure 2). For the 13 mm diameter case, the chain offset dimension (39 mm) and the chain assembly height (42 mm) were approximately three (3) times the nominal diameter of the chain (13 mm). The longitudinal extent of the chain was set between $x = 0$ m (located within the flume inlet zone) and $x = 14.5$ m (100 mm from the channel brink). The anchor chain was lightly tacked to the channel invert with silicone to maintain positional consistency during the experiment.

2.3 | Experimental flow conditions

The physical experiments for the 8 mm diameter and 13 mm diameter anchor chain cases utilized flow rates at 0.015, 0.020, 0.030, 0.040, 0.0556, 0.070, and 0.100 m^3/s for free-surface measurements performed between $x = 0.5$ m and $x = 14.5$ m. Velocity cross-section measurements at $x = 8.0$ m were only conducted at $Q = 0.0556$ m^3/s for the 13 mm diameter anchor chain case, as earlier experiments using an 8 mm diameter anchor chain did not result in a sizable LVZ in the bottom right-hand corner. Consequently, this paper will primarily focus on the results of the 13 mm diameter anchor chain case.

3 | BOX CULVERT BARREL HYDRODYNAMICS

3.1 | Presentation of velocity, Reynolds stress, and TKE results

A culvert comprised three physical flow zones, these being the inlet zone, barrel zone, and outlet zone. In this paper, physical modelling

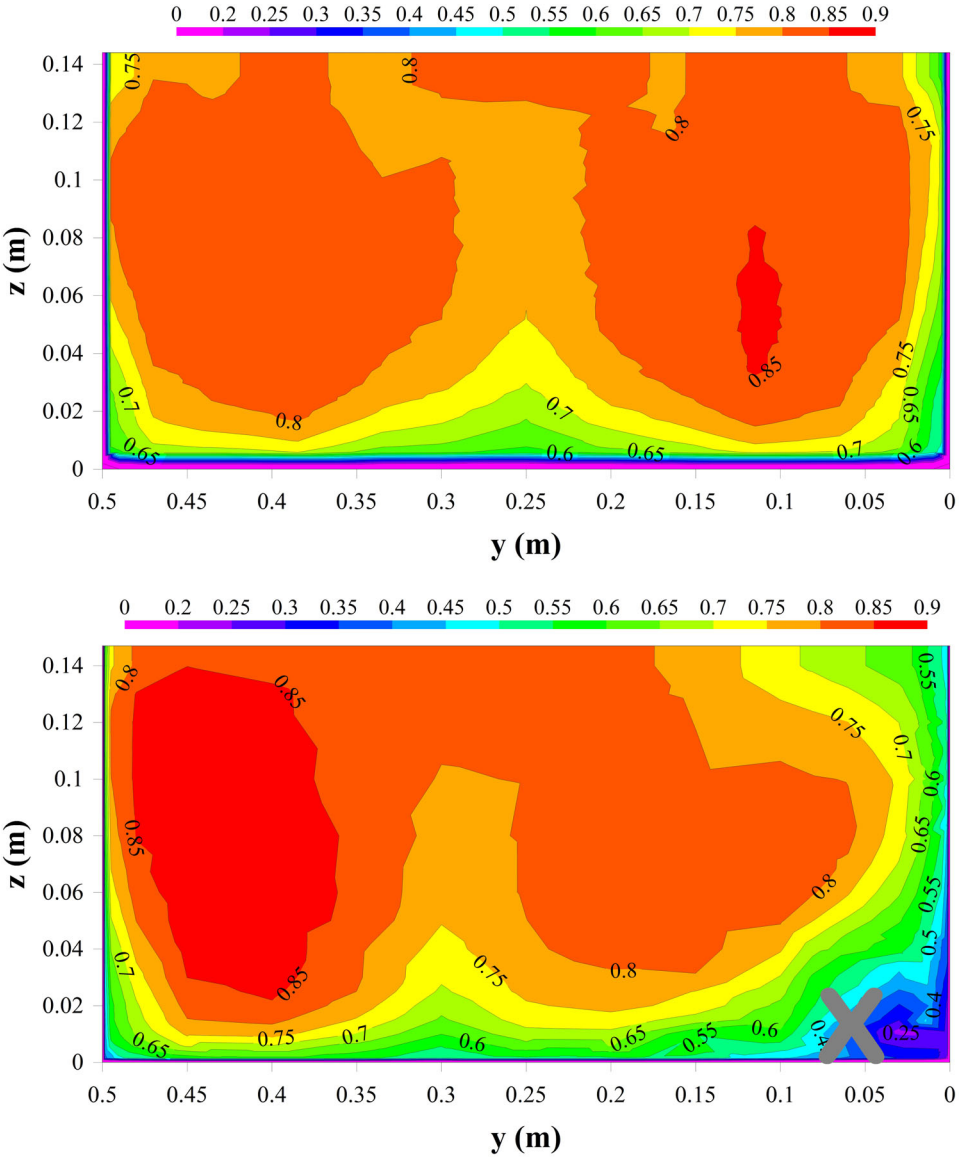

FIGURE 3 Contour maps of time-averaged longitudinal velocity, V_x, $Q = 0.0556$ m^3/s, $x = 8.0$ m. $y = 0.25$ m was the centerline and $y = 0$ m was the right-hand sidewall, velocity scale in m/s, Prandtl Pitot tube, roving Preston tube, and ADV data. (TOP) Smooth rectangular channel, $d = 0.144$ m. (BOTTOM) Smooth rectangular channel fitted with the single 13 mm diameter anchor chain, $d = 0.147$ m. [Color figure can be viewed at wileyonlinelibrary.com]

focused on the culvert barrel zone. The anchor chain was positioned close to the right-hand side wall (streamwise direction). Table 2 highlights the comparison of basic flow results between the smooth rectangular channel and the smooth rectangular channel fitted with a single anchor chain.

Detailed velocity measurements were taken at $x = 8.0$ m for the 13 mm diameter anchor chain case, which was within the fully developed flow zone. For the smooth rectangular channel, the subcritical flow was gradually varied for the full length of the channel. The aspect ratio (B/d) at $x = 8.0$ m was 3.6. According to Nezu and Nakagawa (1993), side channel walls influenced the turbulence flow characteristics at the middle of the flow cross-section for aspect ratios less than five. The outlet was a free brink which induced a H2 free-surface profile (Chanson, 2004). Free-surface undulations were observed within the developing zone ($x = 0$–5 m). The free-surface undulations diminished in the streamwise direction and were marginal at the measurement station ($x = 8$ m). Channel flow was very turbulent with Reynolds number ranging from 329,000 ($x = 0.5$ m) to 374,000 ($x = 14.5$ m). At $x = 8.0$ m, dye injections showed the presence of elongated flow structures, comprising two distinct secondary flow cells. An upwelling zone was also observed at $y = 0.25$ m. These elongated flow structures did not laterally meander to any significant extent. Complex longitudinal streaking was observed, and this was identical to that reported by Imamoto and Ishigaki (1986) during their visualization experiment on a smooth rectangular channel with an aspect ratio of five. Dye injected into both bottom corners remained intact for longitudinal lengths of at least 8–10 times the flow depth, highlighting the presence of low-velocity vortical cells.

For the smooth rectangular channel fitted with a single 13 mm diameter anchor chain, free-surface undulations and very turbulent flow along the channel were also observed. The overall flow depth slightly increased. At $x = 8.0$ m dye injections also showed the presence of two distinct secondary flow cells to the left of the anchor chain and a region of complex flow above the anchor chain. No lateral meandering of secondary flow cells was observed, although dye injections immediately above the anchor chain appeared highly dispersive.

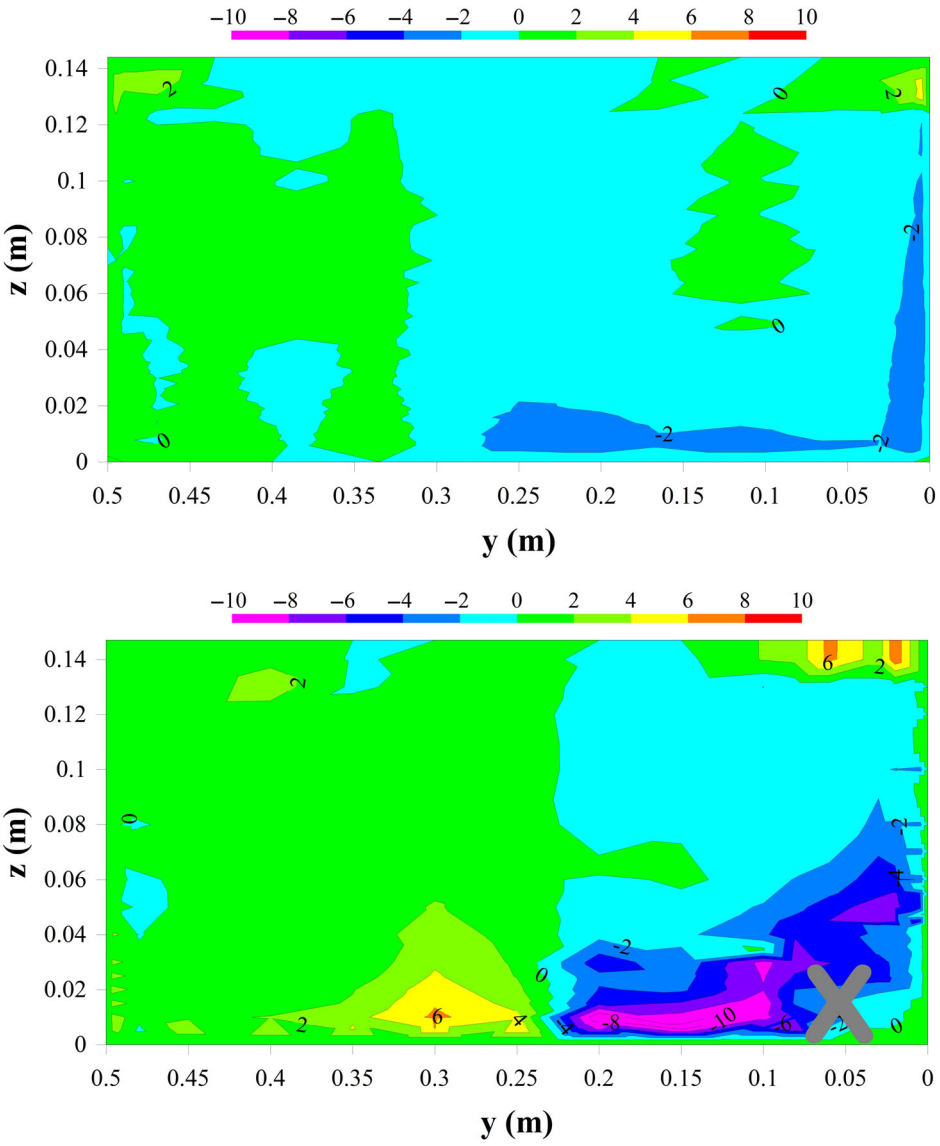

FIGURE 4 Contour maps of Reynolds stress, $\rho \overline{v_x' v_z'}$, $Q = 0.0556\ m^3/s$, $x = 8.0$ m. $y = 0.25$ m was the centerline and $y = 0$ m was the right-hand sidewall, scale in Pa, ADV data. (TOP) Smooth rectangular channel, $d = 0.144$ m. (BOTTOM) Smooth rectangular channel fitted with the single 13 mm diameter anchor chain, $d = 0.147$ m. [Color figure can be viewed at wileyonlinelibrary.com]

Dye injections in the left-hand corner of the channel remained coherent; however, the zone between the anchor chain and the right bottom corner was slightly dispersive. Time-averaged longitudinal velocities were presented in the form of streamwise velocity (V_x) contour maps (Figure 3). The velocity was integrated to check the conservation of mass (Equation 1).

$$\hat{Q} = \sum V_x \Delta A. \quad (1)$$

The integration results closely matched discharge measurements obtained from the Venturi meter to within 0.7% for the smooth rectangular channel and 0.1% for the smooth rectangular channel fitted with a single 13 mm anchor chain. For the smooth rectangular channel case, the streamwise velocity maps generally showed two symmetric high velocity cells. A lower velocity gradient, $\frac{dV_x}{dz}$, was observed at $y = 0.25$ m, and this indicated a zone of upwelling low momentum fluid. Lower velocities were present in the bottom corner zones, which also matched the dye injection observations. For the smooth rectangular channel fitted with a single 13 mm diameter anchor chain, two high velocity cells were observed, although flow asymmetry was notable. A lower velocity gradient, $\frac{dV_x}{dz}$, was observed at the upwelling zone, although this was located at $y = 0.30$ m. Whilst a small LVZ was present in the left bottom corner, a significantly enhanced LVZ was noted in the region between the anchor chain and the right bottom corner.

The instantaneous velocities were measured by ADV velocimeters which allowed for the calculation of turbulent Reynold stresses.

$$\tau'_{ij} = \rho \overline{u'_i u'_j}. \quad (2)$$

The Reynolds stress represents the turbulent flux of momentum within a fluid (Maddock, 2013), and Reynolds stress contour maps for $\rho \overline{v'_x v'_z}$ were presented in Figure 4 for the smooth rectangular channel and the anchor chain configuration. The smooth rectangular channel case showed low magnitudes of Reynolds stress. However, it

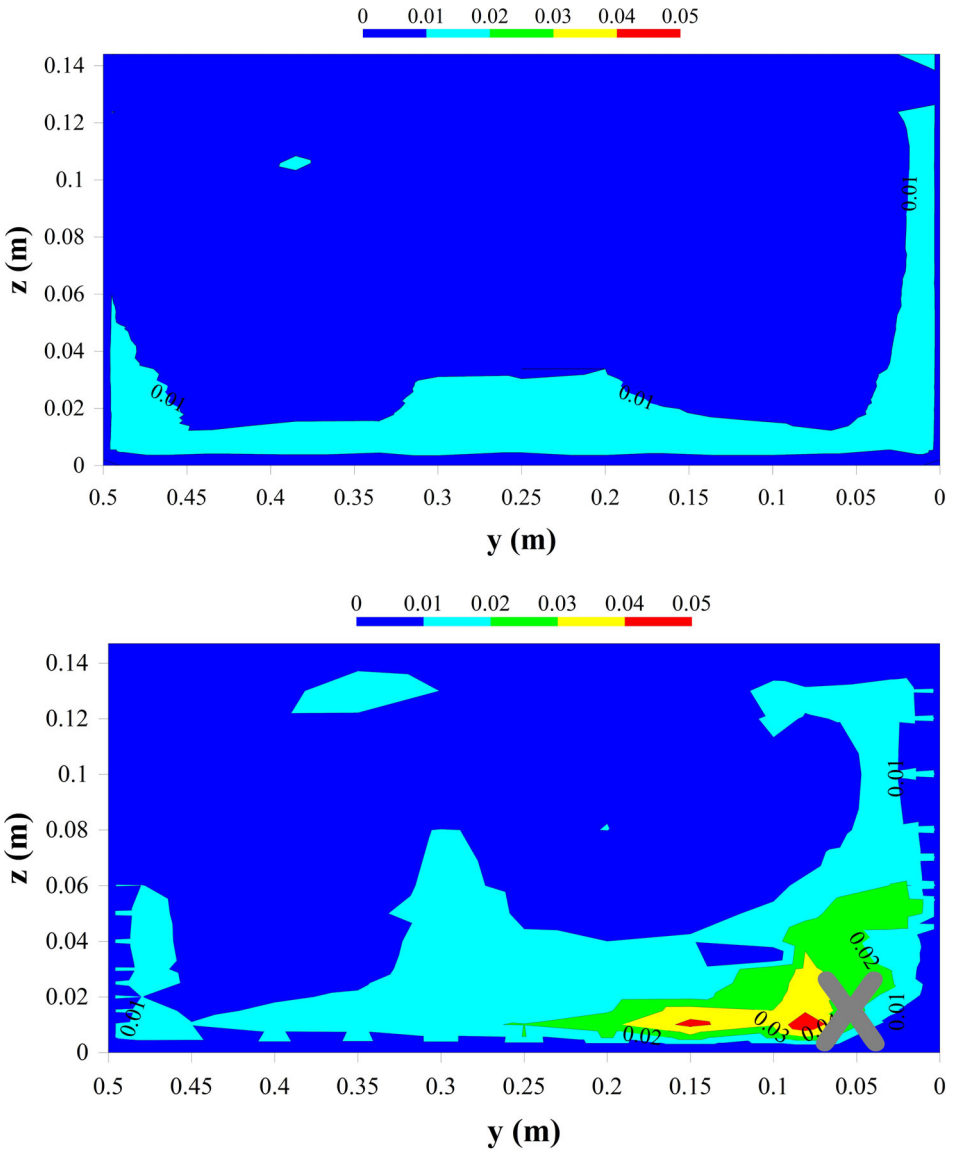

FIGURE 5 Contour maps of turbulent kinetic energy (TKE), $Q = 0.0556$ m^3/s, $x = 8.0$ m. $y = 0.25$ m was the centerline and $y = 0$ m was the right-hand sidewall, scale in m^2/s^2, ADV data. (TOP) Smooth rectangular channel, $d = 0.144$ m. (BOTTOM) Smooth rectangular channel fitted with the single 13 mm diameter anchor chain, $d = 0.147$ m. [Color figure can be viewed at wileyonlinelibrary.com]

should be noted that some Reynolds stress asymmetry appears along the near-wall region within right-hand side of the channel (viewed facing downstream), and it is assessed that this asymmetry may be primarily due to instrument noise despite attempts to minimize acoustic reflectivity in the flume design. For the anchor chain configuration, higher levels of turbulent Reynolds stress were observed at the invert near $y = 0.15$ m. This location was the confluence of the downwelling of secondary flow and bluff body turbulent motion emitted from the anchor chain. The zone between the anchor chain and the right-hand bottom corner showed lower values of Reynolds stress which coincided with the presence of an LVZ. Overall, the turbulent Reynolds stress, $\rho\overline{v_x' v_z'}$, did not exceed the Reynolds stress fish safety threshold of 50 Pa (Odeh et al., 2002).

The turbulent kinetic energy (TKE) contour maps were presented in Figure 5 for the smooth rectangular channel and the anchor chain configuration. The TKE was estimated based on Equation 3 (Dey, 2014).

$$\text{TKE} = \frac{1}{2}\left(\overline{v_x'^2} + \overline{v_y'^2} + \overline{v_z'^2}\right). \quad (3)$$

The smooth rectangular channel case showed low levels of TKE, except in regions close to the wall and invert which showed increased levels of TKE, likely associated with wall-generated turbulence (Dey, 2014). The smooth rectangular channel fitted with a single 13 mm diameter anchor chain presented increased levels of TKE between the centerline ($y = 0.25$ m) and the chain. It was likely that this feature was generated by the presence of the anchor chain and laterally transported towards the upwelling zone at $y = 0.3$ m. Surprisingly, the LVZ near the right-hand bottom corner showed lower levels of TKE despite its proximity to the chain.

3.2 | Friction factors

The flow resistance of the culvert barrel channel was deduced from the free-surface measurements for a range of flows. The standard step method (Chanson, 2004) shown in (Equation 4) was used to calculate the water surface profile from measured depths between $x = 0.5$ m and 14.5 m for $Q = 0.015$, 0.020, 0.030, 0.040, 0.0556, 0.070, and 0.100 m^3/s. The Darcy-Weisbach friction factor calculations relied on the hydraulic diameter, $D_H = 4 \times A/P$, where A is the flow area and P is the wetted perimeter. The Haaland's explicit friction factor formula was used (Haaland, 1983) (Equation 5). Calculated water surface profiles matched measured profiles to within ±0.003 m.

$$\frac{\partial d}{\partial s}\left(1 - Fr^2\right) = S_0 - S_f \text{ where } S_f = \frac{f\, V_{mean}^2}{2g\, D_H}, \quad (4)$$

$$f = \left\{-1.8\log\left[\left(\frac{k_s}{3.7D_H}\right)^{1.11} + \frac{6.9}{Re}\right]\right\}^{-2}, \quad (5)$$

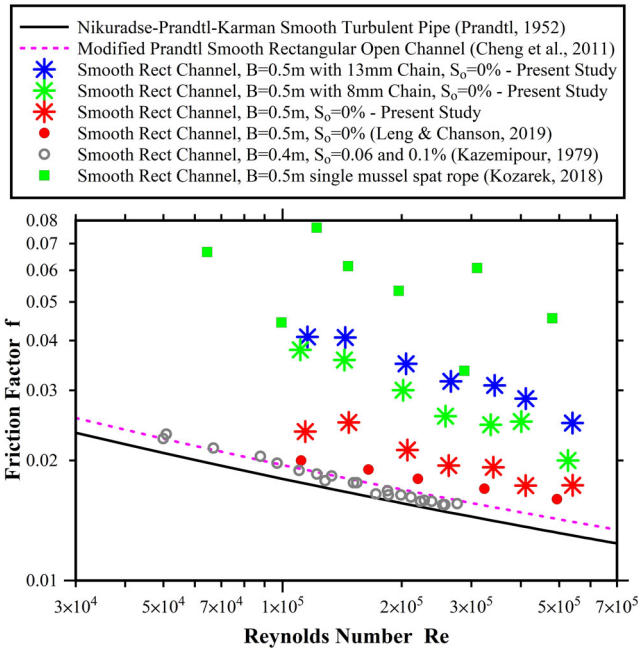

FIGURE 6 Darcy-Weisbach friction factors for smooth rectangular channel at $x = 8.0$ m ($Q = 0.015$, 0.020, 0.030, 0.040, 0.0556, 0.070, and 0.100 m^3/s and $S_0 = 0\%$). Comparison between experimentally derived friction factors, the Nikuradse-Prandtl-Karman smooth turbulent pipe flow formula, modified Prandtl smooth rectangular friction law, and relevant experimental pipe data. (Data from Kazemipour, 1979; Leng & Chanson, 2019; Kozarek & Hernick, 2018). [Color figure can be viewed at wileyonlinelibrary.com]

where

S_f = Friction slope.

k_s = Equivalent sand roughness height.

The results are presented in Figure 6 for the 8 and 13 mm anchor chain configurations. The present data were compared with relevant literature. Whilst the friction factors for the anchor chain configuration were higher than the reference case, friction factors were lower than the single mussel spat rope (Kozarek & Hernick, 2018).

3.3 | Secondary flow

The secondary flow in the smooth rectangular channel comprised two dominant counter-rotating cells spanning the channel centerline (Figure 7). Smaller circulation cells were observed using dye injection in the upper corners, although proximity to the free surface prevented ADV operations. At the channel centerline ($y = 0.25$ m), the counter-rotating circulation cells contributed to the upwelling of fluid from the invert to the free surface, where fluid was eventually redirected to the side walls. This movement contributed to the occurrence of the "velocity dip" (Nezu & Nakagawa, 1993) seen in the longitudinal velocity contour map (Figure 3). The upwelling of fluid at the channel centerline matched the observations from a PIV experiment conducted by Khanarmuei et al. (2020). This experiment was conducted

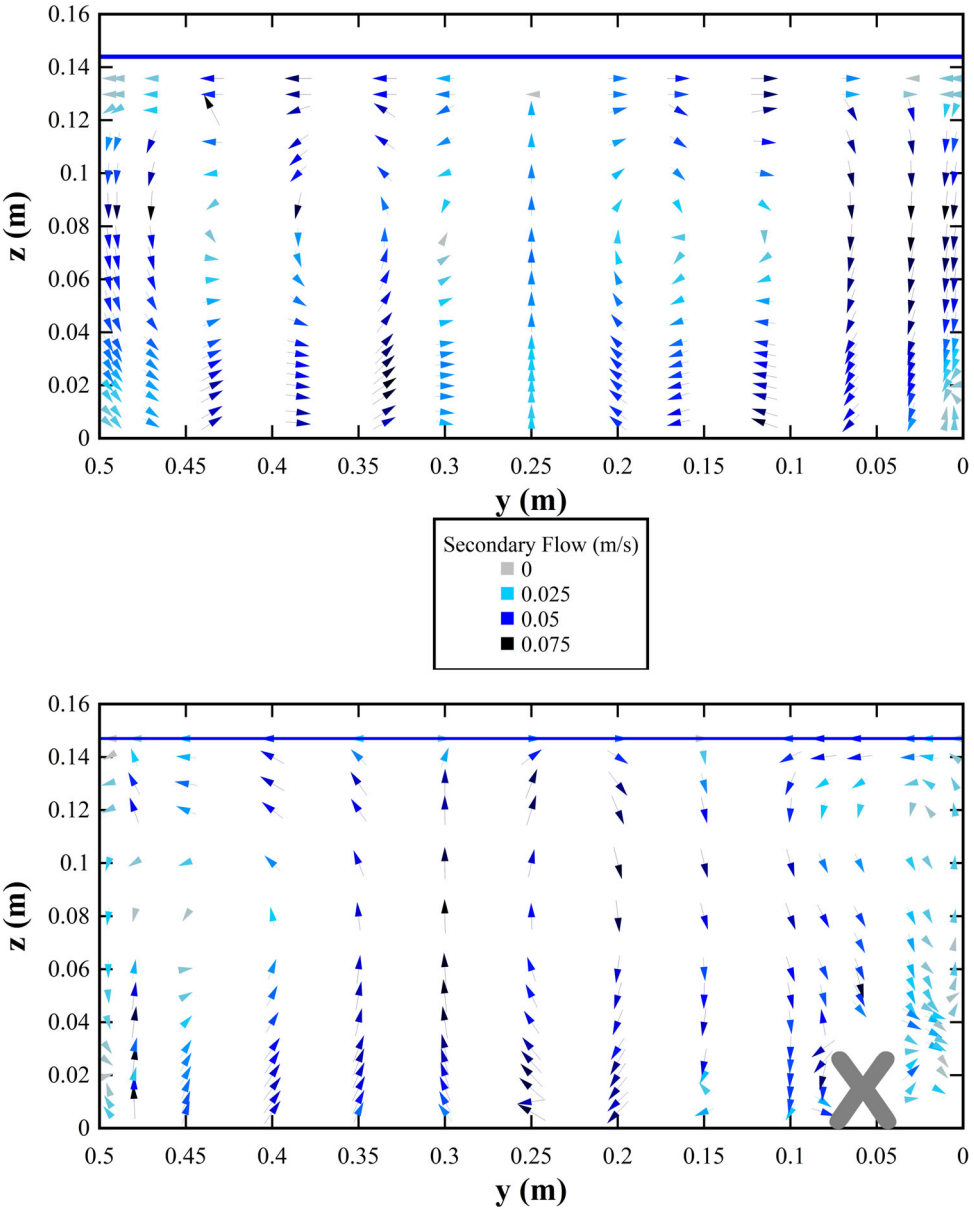

FIGURE 7 Secondary flow maps, $Q = 0.0556\ m^3/s$, $x = 8.0$ m. $y = 0.25$ m was the centerline and $y = 0$ m was the right-hand sidewall, velocity vector plot scaled in m/s, ADV data. Same legend for both graphs. Chain icon removed for clarity. (TOP) Smooth rectangular channel, $d = 0.144$ m. (BOTTOM) Smooth rectangular channel fitted with the single 13 mm diameter anchor chain, $d = 0.147$ m. [Color figure can be viewed at wileyonlinelibrary.com]

on a smooth rectangular channel with an aspect ratio (B/d) of 4. However, their experiments noted three distinct secondary flow circulation cells either side of the centerline upwelling zone, which were similar to the secondary flow streamlines documented by Naot and Rodi (1982). It is believed that these differences were attributed to the experimental flume inflow configuration used in the present study, where inflow into the channel contracted both horizontally and vertically. This created the observed counter-rotating cell patterns, which were transported downstream due to the conservation of angular momentum and the low channel aspect ratio. Dye injections confirmed the presence of a vigorous upwelling of fluid at the centerline and strong counter-rotating cells, at the flume inlet ($x = 0$ m).

The presence of the 13 mm anchor chain significantly modified secondary flow patterns (Figure 7). The anchor chain contributed to the occurrence of a third secondary flow circulation cell above the anchor chain, as well as small-scale weak secondary flow motion in the zone between the anchor chain and the right-hand side wall. Some lateral interchange of fluid within the anchor chain links was evident. This was likely caused by periodic recirculation flow from the chain link acting as a bluff body. Dye injections showed recirculation flow around chain links which also appeared to disperse laterally (Figure 8).

The two dominant counter-rotating secondary flow cells evidenced in the reference case were preserved; however, these secondary flow cells shifted from the anchor chain, with the axis of upwelling fluid movement shifting from $y = 0.25$ m to $y = 0.3$ m. Both cells were strong with secondary flow velocity magnitudes between 8% and 10% of the mean channel velocity, which exceeded the typical magnitudes for rectangular open channels (Nezu & Rodi, 1985; Tominaga et al., 1989). The lateral width of the

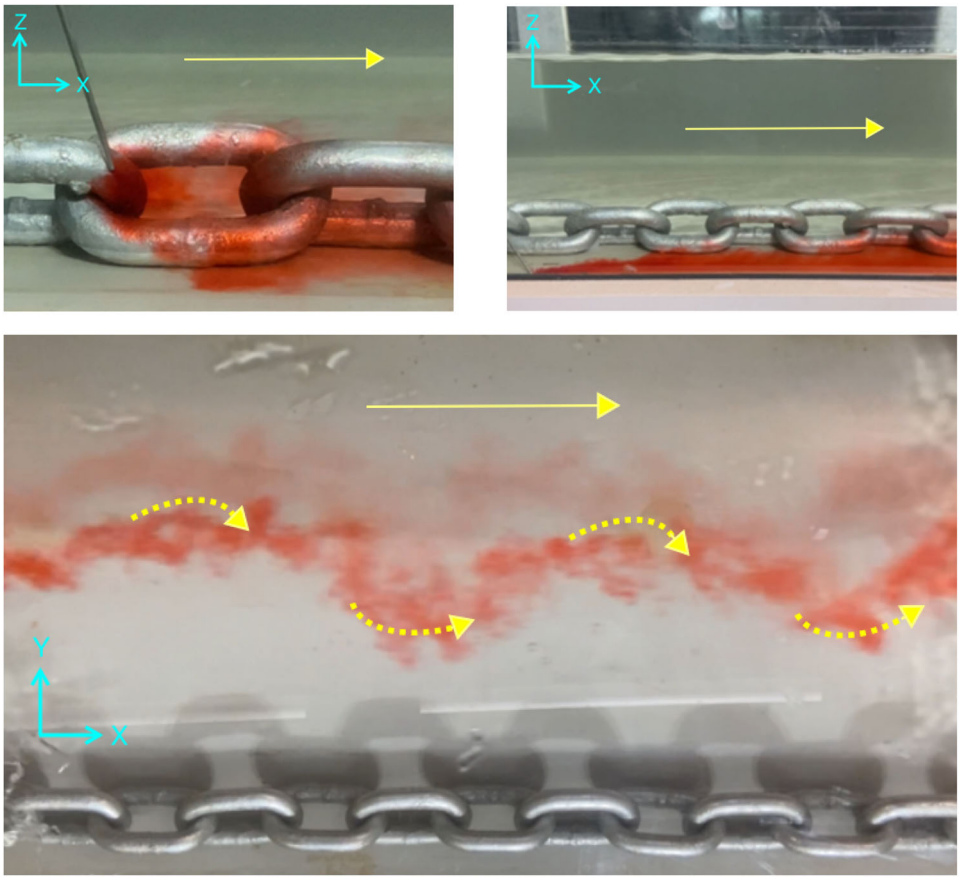

FIGURE 8 Dye injection tests in the smooth rectangular channel fitted with the single 13 mm diameter anchor chain, $Q = 0.0556\ m^3/s$, $x = 10.0$ m. Arrow showed the direction of flow. (TOP LEFT) Dye injection at $y = 0.04$ m showed a recirculating flow pattern in the turbulent wake of a chain link, photograph taken in the direction of the *y* axis. (TOP RIGHT) Dye injection at $y = 0$ m showed a coherent streamline within the LVZ (between the anchor chain and the right-hand sidewall, photograph taken in the direction of the y axis. (BOTTOM) Dye injection at $y = 0.225$ m, $z = 0.05$ m showed the secondary flow vortical cell, photograph taken in the *z* direction (down) (Injection point was not shown in the photograph; however, dye was released at approximately $x = 9.8$ m). [Color figure can be viewed at wileyonlinelibrary.com]

dominant counter-rotating cells was smaller than the reference case. Tamburrino and Gulliver (2007) asserted that lateral flow constraints (such as side walls) tended to suppress the oscillation of streamwise vortices in the spanwise direction. Dye injections confirmed this suppressive effect, with limited spanwise meandering of secondary flow cells.

The vertical protuberance of the 13 mm diameter anchor chain was small (42 mm); however, its complex bluff profile appeared to generate a localized turbulent wake zone capable of reorganizing the original right-hand secondary flow cell into smaller secondary flow cells. Turbulent shear stress gradients created by the anchor chain and the channel corner generated differences in turbulent normal stresses ($v_z'^2 - v_y'^2$) which appeared to be associated with secondary flow (Gerard, 1978; Nezu & Nakagawa, 1993). The difference ($v_z'^2 - v_y'^2$) characterized the generation of streamwise vorticity (Perkins, 1970; Tominaga et al., 1989), and typical results were presented in Figure 9. The contour map of ($v_z'^2 - v_y'^2$) showed that the anchor chain created two distinctly opposing stress gradient zones. To the left of the anchor chain, a strong positive turbulent normal stress gradient close to the channel invert, was associated with the main counter-rotating secondary flow cells between $y = 0.15$ m and 0.45 m. To the right of the anchor chain, a weak negative turbulent normal stress gradient was associated with the right bottom corner LVZ. Above the chain links was a stronger positive turbulent normal stress gradient, associated with the secondary flow cell located in the top right-hand side of the channel.

3.4 | Linking fish morphometrics to low-velocity zones and turbulent flow characteristics

To assess the potential for successful fish passage, the low-velocity zones (LVZ) were matched against the physical body dimensions of target fish species. This was achieved by fitting geometric ellipses to each LVZ in the *yz* plane. Each ellipse represented the main body dimensions of a target fish species. Dimensions were based on the maximum body depth, D_{ma}, and the maximum body width of target fish, W_{ma} (Sagnes & Statzner, 2009). The semi-major axis ellipse length was half the maximum body depth of target fish, and similarly, the semi-minor axis ellipse length was half the maximum body width of target fish (Figure 10). The local time-averaged longitudinal velocity was spatially averaged across the area of the ellipse. This result was denoted as V_{fe} and was subsequently compared with U_{fish} to ensure that the following thresholds were met.

$$V_{fe} < U_{fish}, \tag{6}$$

$$D_{ma} < 2a, \tag{7}$$

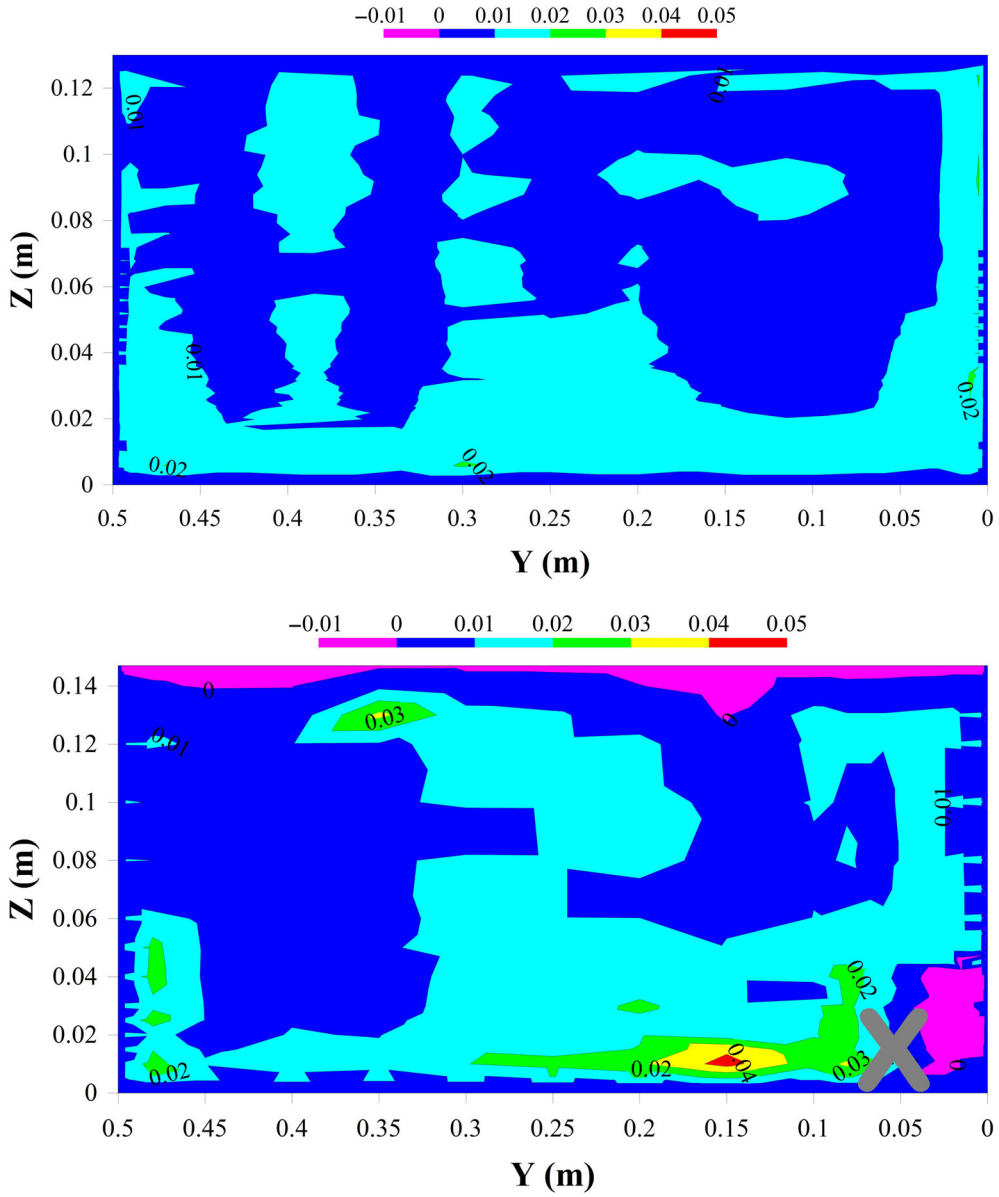

FIGURE 9 Contour maps of the difference $(v_z'^2 - v_y'^2)$, $Q = 0.0556\ m^3/s$, $x = 8.0\ m$, $y = 0.25\ m$ at the centerline and $y = 0\ m$ at the right-hand sidewall, velocity vector plot scaled in m^2/s^2, ADV data. (TOP) Smooth rectangular channel, $d = 0.144\ m$. (BOTTOM) Smooth rectangular channel fitted with the single 13 mm diameter anchor chain, $d = 0.147\ m$. [Color figure can be viewed at wileyonlinelibrary.com]

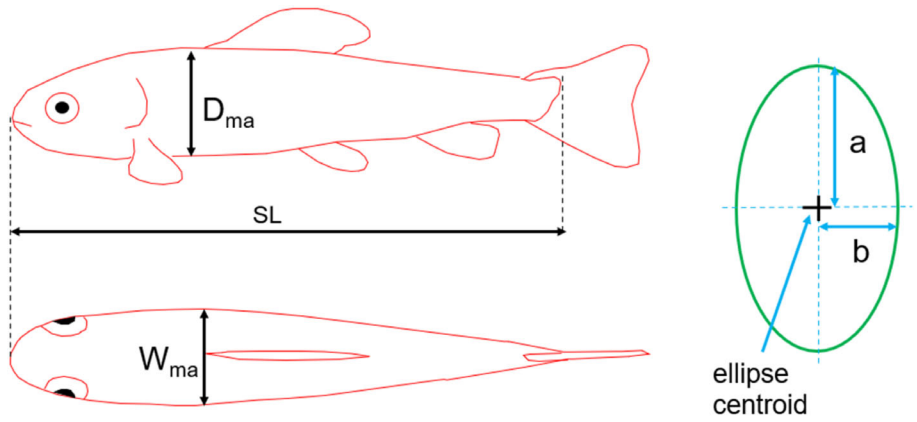

FIGURE 10 Fish morphometrics. (LEFT) Morphometric nomenclature. (RIGHT) Fish ellipse dimensions. [Color figure can be viewed at wileyonlinelibrary.com]

TABLE 3 Summary of target fish characteristic data and target fish ellipse dimensions.

	Standard length, SL (mm)	Body height, D_{ma} (mm)	Body width, W_{ma} (mm)	Target fish ellipse (a × b) (mm)	U_{fish} (m/s)	V_{fe} LVZ (m/s)	Source (S) = speed (D) = dimensions
M. duboulayi	48.8	13.9	9.8	7 × 5	0.44	0.35	Hurst et al. (2007) (S/D); Crowley et al. (1986) (D)
G. gobio	70	13.5	11.6	7 × 6	0.55	0.36	Pavlov et al. (1994) (S); Tudorache et al. (2008) (S/D); Sagnes (1998) (D)
S. trutta fario	78	17.6	13.6	9 × 7	0.65	0.37	Tudorache et al. (2008) (S/D); Sagnes (1998) (D)

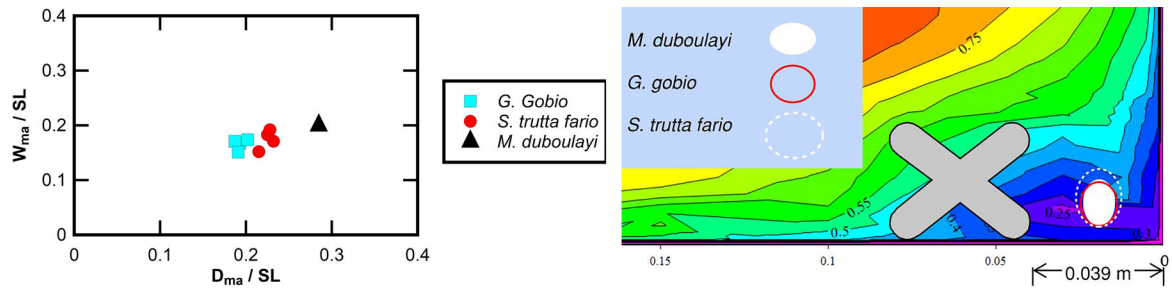

FIGURE 11 (LEFT) Ratio of W_{ma} and D_{ma} with respect to SL. Data for *M. duboulayi* derived from Crowley et al. (1986). Data for *G. gobio* and *S. Trutta fario* derived from Sagnes (1998). (RIGHT) Target fish ellipses applied to the LVZ for *M. duboulayi*, *G. gobio*, and *S. trutta fario* in a smooth rectangular channel with a single 13 mm diameter anchor chain $x = 8.0$ m, $B = 0.5$ m, $Q = 0.0556$ m^3/s. [Color figure can be viewed at wileyonlinelibrary.com]

$$W_{ma} < 2b, \tag{8}$$

where

a = Major semi-axis length of ellipse (mm).

b = Minor semi-axis length of ellipse (mm).

D_{ma} = Maximum body depth of target fish (mm).

W_{ma} = Maximum body width of target fish (mm).

V_{fe} = Average longitudinal velocity within the ellipse (m/s), where $V_{fe} = \int_A \overline{v_x}\, dA$.

$\overline{v_x}$ = Time-averaged local longitudinal velocity (m/s).

U_{fish} = Characteristic fish speed (m/s) dictated by the relevant fish management agency, which is typically based on U_{crit} values.

The anatomical features of fish such as dorsal and pelvic fins were not included in the ellipse sizing. Figure 10 graphically shows the basic dimensional nomenclature for fish and representative ellipses.

Three species of common small-bodied riverine fish were considered in this paper. Firstly, the Crimson-Spotted Rainbow Fish *Melanotaenia duboulayi*, endemic to coastal streams of south-east Queensland, Australia. *M. duboulayi* juveniles were typically 20 mm long at 8 weeks age, whilst adults in the wild grew to 90 mm long (Pusey et al., 2004). Swim tests in laboratory flumes showed that *M. duboulayi*, with a mean total length of 48.8 mm ± 1.8 mm, had a $U_{fish} = 0.44$ m/s (Hurst et al., 2007). This study data compared well with sub-adults (age 1–2 years) that represented the dominant age class in common stream populations (Milton & Arthington, 1984; Pusey et al., 2004). Secondly, the Gudgeon, *Gobio gobio*, were found in freshwater systems in Europe and Western Asia. Specimens had a long slender round body shape and a total length usually less than 120 mm. Experiments showed that *G. gobio* had a U_{fish} ranging between 0.32 and 0.60 m/s depending on length (Pavlov et al., 1994; Tudorache et al., 2008). Finally, the Brown Trout, *Salmo trutta fario*, a predatory fish originating from Europe, was an introduced species in many locations worldwide. Despite large adults attaining high fish speeds, smaller juveniles are vulnerable to high culvert velocities. Experiments showed that juvenile *S. trutta fario*, with a total length of 78 mm, had a U_{fish} of 0.65 m/s (Tudorache et al., 2008). The maximum body depths, D_{ma}, and maximum body widths, W_{ma}, were expressed as a ratio of standard fish length, SL, and were detailed in Figure 10. The mean values of these ratios were used to size the target fish ellipse. Based on Figure 3, the LVZ between the anchor chain and the right-hand bottom corner was selected. Target fish ellipses were then calculated based on Equations (6), (7), and (8). The values for U_{fish} were greater than V_{fe} and appeared to be suitable for the target fish species. Whilst V_{fe} was a spatially-averaged velocity, estimated as part of this study, and U_{fish} was typically based on U_{crit} data from laboratory experiments involving near-uniform velocity profiles, the results shown in Table 3 indicated prima-facie support for upstream fish passage.

Figure 11 showed the location of target fish ellipses in relation to the velocity gradients located near the invert and the anchor chain.

The integral turbulent time scales, T_{Ei}, were calculated using time series data collected from the acoustic Doppler velocimeter based on the following equation (Chanson, 2014).

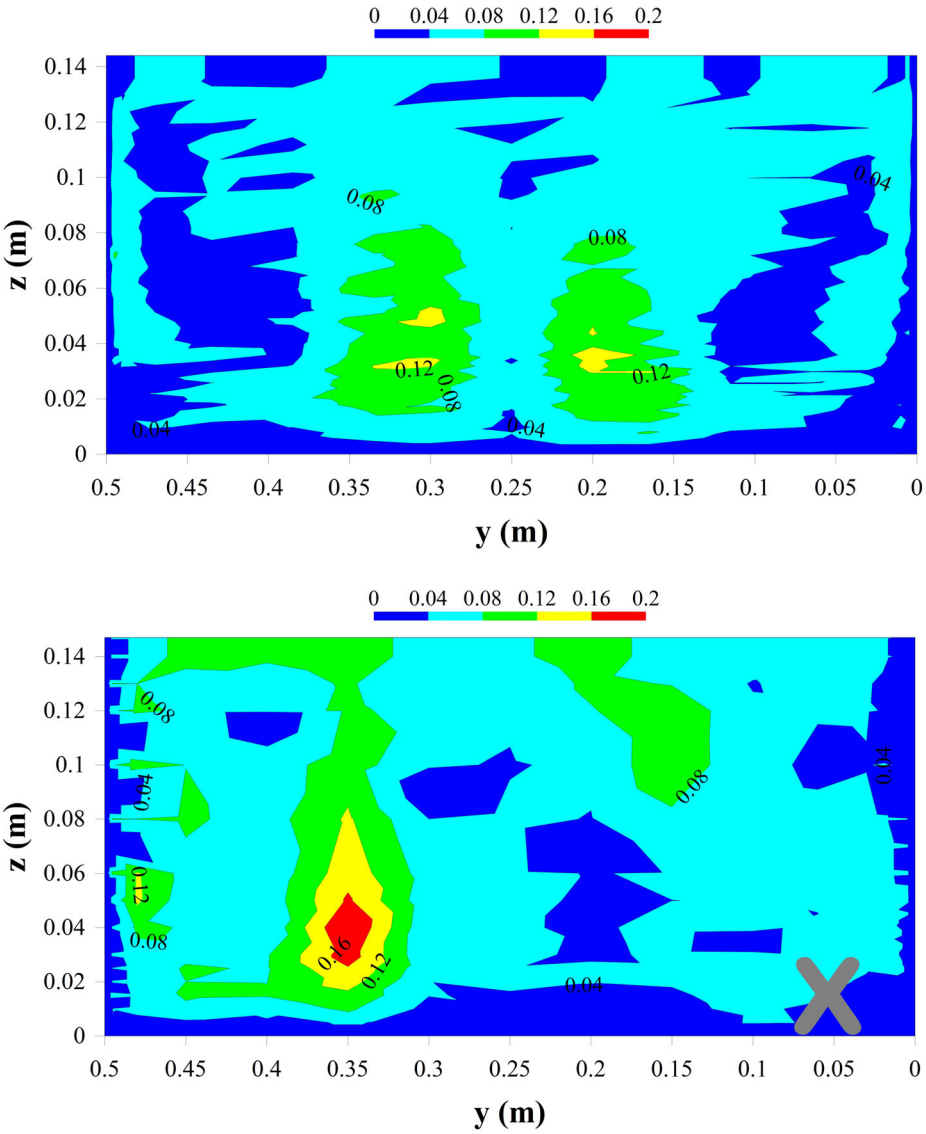

FIGURE 12 Contour maps of the integral scales length (L_x), $Q = 0.0556\ m^3/s$, $x = 8.0$ m. $y = 0.25$ m was the centerline and $y = 0$ m was the right-hand sidewall, scale in m, based on ADV data. (TOP) Smooth rectangular channel, $d = 0.144$ m. (BOTTOM) Smooth rectangular channel fitted with the single 13 mm diameter anchor chain, $d = 0.147$ m. [Color figure can be viewed at wileyonlinelibrary.com]

$$T_{Ei} = \int_0^{\tau(R_{ii}=0)} R_{ii}(\tau)\, d\tau, \tag{9}$$

where $R_{ii}(\tau)$ is the normalized autocorrelation function, $R_{ii}(\tau) = \frac{\overline{v_i(t)\, v_i(t+\tau)}}{\overline{v_i^2}}$.

Integral length scales, L_x, were then calculated by applying Taylor's frozen hypothesis, based on the following relationship (Hinze, 1975).

$$L_x = \overline{V_x}\, T_{Ex}. \tag{10}$$

Results for the smooth rectangular channel showed the presence of large energetic length scales, of similar magnitude to the flow depth, coinciding with the presence of high velocity zones (Figure 12). Smaller scales (L_x <0.04 m) were present in both bottom corners. In comparison, the chain configuration showed a distinct asymmetrical distribution of length scales. The larger energetic scales were concentrated and intensified within the left-hand high velocity cell, whilst a reduction of length scales was noted in the right-hand high velocity cell. The extent of smaller scales (L_x <0.04 m) in the bottom left-hand corner was reduced; however, the bottom right-hand corner remained relatively unchanged.

The proportion of length scale (L_x) to fish length (SL) was critical for the stability of fish. Lupandin (2005) reported that eddy sizes over 66% of the fish length may destabilize a fish, whilst Tritico and Cotel (2010) stated that this ratio was 75%. Consequently, small-bodied mass fish may be adversely affected by L_x, subject to other turbulence characteristics (Maddock, 2013). The ratio of the target fish length (SL) to the integral length scale (L_x) showed the suitability of target fish species to specific locations within the channel cross-section (Figure 13). In particular, the LVZ (between the anchor chain and the right-hand bottom corner) appeared to be suitable for all fish species investigated in this paper.

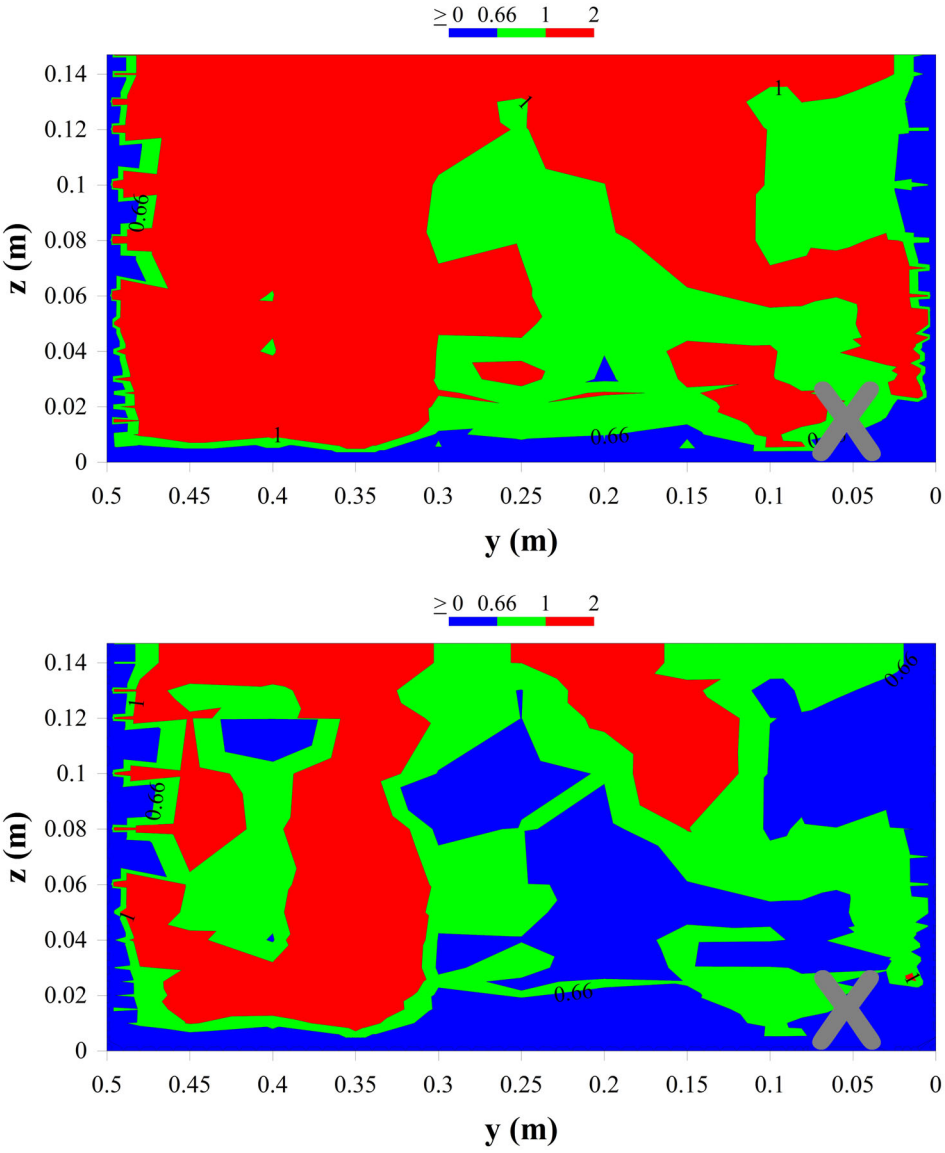

FIGURE 13 Contour maps of the ratio of fish length (FL) to integral scales length (L_x) in the smooth rectangular channel fitted with the single 13 mm diameter anchor chain, $Q = 0.0556\ m^3/s$, $x = 8.0$ m, $d = 0.147$ m. $y = 0.25$ m was the centerline and $y = 0$ m was the right-hand sidewall, FL / L_x non-dimensional scale, based on ADV data. (TOP) *M. duboulayi*. (BOTTOM) *G. gobio*. [Color figure can be viewed at wileyonlinelibrary.com]

4 | CONCLUSION

This study aims to enhance the upstream passage of small-bodied and juvenile fish in smooth rectangular box culverts. The physical investigations were conducted for a range of flow rates corresponding to less-than-design flows for a subcritical open channel flow in a smooth box culvert barrel with a flat slope, although the impact of boundary treatments on fish performance was not tested. A smooth rectangular channel was used as the reference configuration. The study then primarily investigated a simple solution, a single 13 mm diameter anchor chain fitted to the invert, located 39 mm from the right-hand sidewall.

The small anchor chain generated some flow asymmetry, as well as enhancing the LVZ located between the anchor chain and the right-hand bottom channel corner. Some strong secondary flow was observed above the anchor chain as well as in the middle of the channel. The secondary flow structure was markedly different between the smooth boundary treatment and the configuration with single 13 mm diameter anchor chain. The distributions of turbulent kinetic energy and normal turbulent stresses ($v_z'^2 - v_y'^2$) showed distinct differences between each boundary treatment, with the position of the anchor chain inducing secondary flow motion. Consequently, these motions formed LVZs which could support the upstream movement of small-bodied mass fish. The anchor chain created a third secondary flow zone which enhanced the LVZ located on the bottom right-hand corner. The anchor chain resulted in a modest increase in flow resistance. Consequently, culvert barrel design roughness coefficients must be increased to account for the presence of the anchor chain.

Finally, the proposed anchor chain device still requires field verification, and refinements may be necessary. However, at this stage, the anchor chain appears to be a simple low-cost fish passage solution for new and retrofit box culverts in both advanced and developing countries.

ACKNOWLEDGMENTS

The authors acknowledge Dr. Pierre Sagnes (Institute of Fluid Mechanics, Toulouse) for valuable data input concerning fish

morphology and Ensilon Consulting Australia for construction cost data on fish passage devices. The authors also acknowledge the technical assistance of Jason Van Der Gevel and Stewart Matthews (The University of Queensland). The financial support of the University of Queensland, School of Civil Engineering, is acknowledged. In line with recommendations of the Office of the Commonwealth Ombudsman (Australia) and International Committee on Publication Ethics (COPE), Hubert Chanson has a conflict of interest with Craig E. Franklin. Open access publishing facilitated by The University of Queensland, as part of the Wiley - The University of Queensland agreement via the Council of Australian University Librarians.

FUNDING INFORMATION

The financial support of the University of Queensland, School of Civil Engineering, is acknowledged.

CONFLICT OF INTEREST STATEMENT

Jason Harley and Hui Ling Wong have no conflict of interest nor competing interest. In line with recommendations of the Office of the Commonwealth Ombudsman (Australia) and International Committee on Publication Ethics (COPE), Hubert Chanson has a conflict of interest with Craig E. Franklin.

DATA AVAILABILITY STATEMENT

The data that support the findings of this study are available from the corresponding author upon reasonable request.

ORCID

Jason Harley https://orcid.org/0000-0003-1869-3362
Hui Ling Wong https://orcid.org/0000-0001-6624-7231
Hubert Chanson https://orcid.org/0000-0002-2016-9650

REFERENCES

Ball, J., Babister, M., Nathan, R., Weeks, W., Weinmann, E., Retallick, M., & Testoni, I. (Eds.). (2019). Australian rainfall and runoff: A guide to flood estimation, Commonwealth of Australia, Geoscience Australia.

Beamish, F. (1978). Swimming capacity. In D. Hoar & W. Randall (Eds.), *Fish physiology* (pp. 101–187). Academic Press.

Birnie-Gauvin, K., Franklin, P., Wilkes, M., & Aarestrup, K. (2019). Moving beyond fitting fish into equations: Progressing the fish passage debate in the Anthropocene. *Aquatic Conservation: Marine and Freshwater Ecosystems*, *29*(7), 1095–1105.

British Standard. (1943). Flow measurement. In *British Standard code BS 1042:1943*. British Standard Institution.

Cabonce, J., Fernando, R., Wang, H., & Chanson, H. (2019). Using small triangular baffles to facilitate upstream fish Passage in Standard box culverts. *Environmental Fluid Mechanics*, *19*(1), 157–179. https://doi.org/10.1007/s10652-018-9604-x

Cabonce, J., Wang, H., & Chanson, H. (2018). Ventilated corner baffles to assist upstream Passage of small-bodied fish in box culverts. *Journal of Irrigation and Drainage Engineering*, *144*(8), 8. https://doi.org/10.1061/(ASCE)IR.1943-4774.0001329

Chanson, H. (2004). *The hydraulics of Open Channel flow: An Introduction* (2nd ed., p. 630). Butterworth Heinemann.

Chanson, H. (2014). *Applied hydrodynamics: An Introduction* (p. 448). CRC Press/Balkema, Taylor & Francis Group, Leiden.

Chanson, H. (2020). Low Velocity Zone in Smooth Pipe Culvert with and without Streamwise Rib for, Low-Velocity Zone in Smooth Pipe Culvert with and without Streamwise Rib for Fish Passage.

Chanson, H., & Leng, X. (2019). There is something fishy about turbulence: Why novel hydraulic engineering guidelines can assist the upstream passage of small-bodied fish species in standard box culverts. *Civil Engineering Research Bulletin No. 26*. School of Civil Engineering, The University of Queensland, Brisbane, Australia. 224.

Chanson, H., & Leng, X. (2021). *Fish swimming in turbulent waters. Hydraulics guidelines to assist upstream fish Passage in box culverts* (p. 202). CRC Press, Taylor and Francis Group. https://doi.org/10.1201/9781003029694

Chanson, H. (2020). Low-velocity zone in smooth pipe culvert with and without streamwise rib for fish passage. *Journal of hydraulic engineering, ASCE*, *146*(9), 10. https://doi.org/10.1061/(ASCE)HY.1943-7900.0001789

Cheng, N., Nguyen, H., Zhao, K., & Tang, X. (2011). Evaluation of flow resistance in smooth rectangular open channels with modified Prandtl friction law. *Journal of Hydraulic Engineering*, *137*(4), 441–450.

Crowley, L., Ivantsoff, W., & Allen, G. (1986). Taxonomic position of two crimson-spotted rainbowfish, *Melanotaenia duboulayi* and *Melanotaenia fluviatilis* (Pisces: Melanotaeniidae), from eastern Australia, with special reference to their early life-history stages. *Australian Journal of Marine and Freshwater Research*, *37*, 385–398.

David, B., Hamer, M., & Collier, K. (2009). Mussel spat ropes provide passage for banded kokopu (*Galaxias fasciatus*) in laboratory trials. *New Zealand Journal of Marine and Freshwater Research*, *43*(4), 883–888. https://doi.org/10.1080/00288330909510046

David, B., Tonkin, J., Taipeti, K., & Hokianga, H. (2014). Learning the ropes: Mussel spat ropes improve fish and shrimp passage through culverts. *Journal of Applied Ecology*, *51*(1), 214–223.

Department of Agriculture & Fisheries. (2018). *Accepted development requirements for operational work that is constructing or raising waterway barrier works*. State of Queensland.

Dey, S. (2014). *Fluvial hydrodynamics*. Springer-Verlag.

Enders, E., Boisclair, D., & Roy, A. (2003). The effect of turbulence on the cost of swimming for juvenile Atlantic salmon (*Salmo salar*). *Canadian Journal of Fisheries and Aquatic Sciences*, *60*(9), 1149–1160.

Ensilon Consulting. (2024). Personal communication, January 14, 2024.

Gerard, R. (1978). Secondary flow in noncircular conduits. *Journal of Hydraulic Division, ASCE*, *104*(HY5), 755–773.

Gessner, F. B. (1973). The origin of secondary flow in turbulent flow along a corner. *Journal of Fluid Mechanics*, *58*(Part 1), 1–25.

Goerig, E., Castro-Santos, T., & Bergeron, N. (2016). Brook trout passage performance through culverts. *Canadian Journal of Fisheries and Aquatic Sciences*, *73*(1), 94–104.

Goettel, M., Atkinson, J., & Bennett, S. (2015). Behavior of western blacknose dace in a turbulence modified flow field. *Ecological Engineering*, *74*, 230–240.

Goring, D., & Nikora, V. (2002). Despiking acoustic Doppler Velocimeter data. *Journal of hydraulic engineering*, *128*(1), 117–126.

Haaland, S. (1983). Simple and explicit formulas for the friction factor in turbulent pipe flow. *Journal of Fluids Engineering*, *105*, 89–90.

Hinze, J. (1975). *Turbulence* (2nd ed.). McGraw-hill.

Humphries, P., & Walker, K. (2013). *Ecology of Australian freshwater fishes* (p. 436). CSIRO Publishing.

Hurst, T., Kay, B., Ryan, P., & Brown, M. (2007). Sublethal effects of mosquito larvicides on swimming performances of larvivorous fish *Melanotaenia duboulayi* (Atheriniformes: Melanotaeniidae). *Journal of Economic Entomololy*, *100*(1), 61–65.

Imamoto, H., & Ishigaki, T. (1986). Visualization of longitudinal eddies in an Open Channel flow. In *Proc. 4th international symposium on flow visualization*, 26–29 Aug. (pp. 333–337). Kyoto University.

Jones, M., & Hale, R. (2020). Using knowledge of behaviour and optic physiology to improve fish passage through culverts. *Fish and Fisheries*, *21*(3), 557–569.

Kapitzke, I. R. (2010). Culvert fishway planning and design guidelines. In *Stage 1-project based guidelines: Part E–fish passage design site scale*. James Cook University.

Katopodis, C. (1992). *Introduction to Fishway design*. Freshwater Institute, Central and Arctic Region, Department of Fisheries and Oceans.

Kazemipour, A. (1979). *Cross-sectional shape effects on resistance to uniform flow in open channels and non-circular closed conduits*. Ph.D. thesis, (p. 462). The University of Queensland, Department of Civil Engineering.

Khanarmuei, M., Akutina, Y., Dupuis, V., Eiff, O., Trevisson, M., Suara, K., & Brown, R. (2020). Secondary currents in smooth-wall open channel flow. In *River flow 2020: Proceedings of the 10th conference on fluvial hydraulics (Delft, Netherlands)* (p. 47). CRC Press.

Kozarek, J., & Hernick, M. (2018). Use of mussel spat rope for fish Passage in culverts—research project final report 2018–13, St. Anthony Falls Laboratory, University of Minnesota. Retrieved May 13th, 2024, from: https://conservancy.umn.edu/handle/11299/197457

Lacey, R., Neary, V., Liao, J., Enders, E., & Tritico, H. (2012). The IPOS framework: Linking fish swimming performance in altered flows from laboratory experiments to rivers. *River Research and Applications*, *28*, 429–443.

Larinier, M. (2002). Fish Passage through culverts, rock weirs and estuarine obstructions. *Bulletin Français de Pêche et Pisciculture*, *364*(364 Supplement), 119–134.

Leng, X., & Chanson, H. (2019). Physical modelling of sidewall baffles in Standard box culvert barrel to assist upstream fish Passage. In *Hydraulic Model Report No. CH115/19 School of Civil Engineering* (p. 87). The University of Queensland.

Leng, X., & Chanson, H. (2020). Full-height sidewall baffles in box culvert to assist upstream fish passage: Physical modelling. 8th IAHR International Symposium on Hydraulic Structures ISHS2020, Santiago, Chile, 12-15 May 2020.

Li, Y., & Chanson, H. (2020). Hydrodynamic instabilities in open-channel flow past lateral cavities. *22nd Australasian Fluid Mechanics Conference, AFMC 2020*, 1–4.

Li, Z., Harley, J., & Chanson, H. (2022). Physical modelling of pipe culverts to assist upstream fish passage. *River Research and Applications*, *38*(2), 309–322.

Liao, J. (2007). A review of fish swimming mechanics and behaviour in altered flows. *Philosophical Transactions of the Royal Society B*, *362*, 1973–1993.

Lupandin, A. (2005). Effect of flow turbulence on swimming speed of fish. *Biology Bulletin*, *32*, 461–466.

Lynch, A., Cooke, S., Deines, A., Bower, S., Bunnell, D., Cowx, I., & Beard, T., Jr. (2016). The social, economic, and environmental importance of inland fish and fisheries. *Environmental Reviews*, *24*(2), 115–121.

Maddock, I. (2013). *Ecohydraulics: An integrated approach*. John Wiley & Sons.

Marsden, T. (2015). OceanWatch Australia: Culvert fish Passage. Report to OceanWatch Australia. Australasian Fish Passage Services, 36pp.

Miles, N., Walsh, C., Bulter, G., Ueda, H., & West, R. (2013). Australian diadromous fishes–challenges and solutions for understanding migrations in the 21st century. *Marine and Freshwater Research*, *65*(1), 12–24.

Milton, D., & Arthington, A. (1984). Reproductive strategy and growth of the crimson-spotted rainbowfish, *Melanotaenia splendida fluviatilis* (Castelnau) (Pisces: Melanotaeniidae) in south-eastern Queensland. *Australian Journal of Marine and Freshwater Research*, *35*, 75–83.

Naot, D., & Rodi, W. (1982). Calculation of secondary currents in channel flow. *Journal of Hydraulic Division, ASCE*, *108*(HY8), 948–967.

Nezu, I., & Nakagawa, H. (1993). Turbulence in Open-Channel flows. IAHR Monograph, IAHR Fluid Mechanics Section, Balkema Publ., Rotterdam, The Netherlands, 281 pp.

Nezu, I., & Rodi, W. (1985). Experimental study on secondary currents in open channel flow. *21st IAHR Congress, Melbourne*, Australia, 19–23 August 1985.

Odeh, M., Noreika, J., Haro, A., Maynard, A., Castro-Santos, T., & Cada, G. (2002). Evaluation of the effects of turbulence on the behavior of migratory fish, report prepared for the U.S. Department of Energy, Bonneville power administration, division of fish and wildlife, U.S. Geological Survey and Oak Ridge National Laboratory.

Pavlov, D., Lupandin, A., & Skorobogatov, M. (1994). Influence of flow turbulence on critical flow velocity for gudgeon (*Gobio gobio*). *Doklady Biological Sciences*, *336*, 215–217.

Pavlov, D., Lupandin, A., & Skorobogatov, M. (2000). The effects of flow turbulence on the behavior and distribution of fish. *Journal of Ichthyology*, *40*(S2), 232–261.

Perkins, H. (1970). The formation of streamwise vorticity in turbulent flow. *Journal of Fluid Mechanics*, *44*(Part 4), 721–740.

Pusey, B., Kennard, M., & Arthington, A. (2004). *Freshwater fishes of north-eastern Australia*. CSIRO Publishing.

Rajaratnam, N., & Katopodis, C. (1990). Hydraulics of culvert Fishways III: Weir baffle culvert Fishways. *Canadian Journal of Civil Engineering*, *17*, 558–568.

Rajaratnam, N., Katopodis, C., & Lodewyk, S. (1988). Hydraulics of offset baffle culvert Fishways. *Canadian Journal of Civil Engineering*, *15*, 1043–1051.

Rajaratnam, N., Katopodis, C., & Lodewyk, S. (1991). Hydraulics of culvert Fishways IV: Spoiler baffle culvert Fishways. *Canadian Journal of Civil Engineering*, *18*, 76–82.

Rajaratnam, N., Katopodis, C., & McQuitty, N. (1989). Hydraulics of culvert Fishways II: Slotted weir culvert Fishways. *Canadian Journal of Civil Engineering*, *16*, 375–383.

Rodgers, E., Cramp, R., Gordos, M., Weier, A., Fairfall, S., Riches, M., & Franklin, C. (2014). Facilitating upstream passage of small-bodied fishes: Linking the thermal dependence of swimming ability to culvert design. *Marine and Freshwater Research*, *65*(8), 710–719.

Rolls, R., Ellison, T., Faggotter, S., & Roberts, D. (2013). Consequences of connectivity alteration on riverine fish assemblages: Potential opportunities to overcome constraints in applying conventional monitoring designs. *Aquatic Conservation: Marine and Freshwater Ecosystems*, *23*(4), 624–640.

Sagnes, P. (1998). *Morphométrie, potentiel hydrodynamique et utilisation de l'habitat lotique par les poissons: une nouvelle approche écomorphologique. PhD Thesis*. Université Lyon I.

Sagnes, P., & Statzner, B. (2009). Hydrodynamic abilities of riverine fish: A functional link between morphology and velocity use. *Aquatic Living Resources*, *22*(1), 79–91.

Sanchez, P., Leng, X., Von Brandis-Martini, J., & Chanson, H. (2020). Hybrid modelling of low velocity zones in an Asymmetrical Channel with sidewall longitudinal rib to assist fish Passage. *River Research and Applications*, *36*(5), 807–818.

Sanchez, P. X., Leng, X., & Chanson, H. (2018). Fluid dynamics and secondary currents in an asymmetrical Rectangular Canal with sidewall Streamwise rib. Hydraulic Model Report No. CH113/18, School of Civil Engineering, The University of Queensland, Brisbane, Australia, 158 pages (ISBN 978-1-74272-223-8).

Shoemaker, R. (1956). *Hydraulics of box culverts with fish-ladder baffles*. Engineering Experiment Station.

Silva, A., Lucas, M., Castro-Santos, T., Katopodis, C., Baumgartner, L., Thiem, J., & Cooke, S. (2018). The future of fish passage science, engineering, and practice. *Fish and Fisheries*, *19*(2), 340–362.

Smith, D., Brannon, E., & Odeh, M. (2005). Response of juvenile rainbow trout to turbulence produced by prismatoidal shapes. *Transactions of the American Fisheries Society*, *134*(3), 741–753.

Standards Australia. (2004). AS 4177.4-2004 Caravan and light trailer towing components—Part 4: Safety chains up to 3500 kg capacity. Sydney.

Starrs, D., Ebner, B., Lintermans, M., & Fulton, C. (2011). Using sprint swimming performance to predict upstream passage of the endangered Macquarie perch in a highly regulated river. *Fisheries Management and Ecology*, *18*(5), 360–374.

Stuart, I., & Mallen-Cooper, M. (1999). An assessment of the effectiveness of a vertical-slot fishway for non-salmonid fish at a tidal barrier on a large tropical/subtropical river. *Regulated Rivers: Research & Management:An International Journal Devoted to River Research and Management*, *15*(6), 575–590.

Tamburrino, A., & Gulliver, J. (2007). Free-surface visualization of Streamwise vortices in a channel flow. *Water Resources Research*, *43*, p12.

Tominaga, A., Nezu, I., Ezaki, K., & Nakagawa, H. (1989). Three-dimensional turbulent structure in straight open channel flows. *Journal of Hydraulic Research, IAHR*, *27*(1), 149–173.

Tonkin, J., Wright, L., & David, B. (2012). Mussel spat ropes assist Redfin bully *Gobiomorphus huttoni* Passage through experimental culverts with velocity barriers. *Water*, *4*, 683–689.

Tritico, H., & Cotel, A. (2010). The effects of turbulent eddies on the stability and critical swimming speed of creek chub (*Semotilus atromaculatus*). *Journal of Experimental Biology*, *213*, 2284–2293.

Tudorache, C., Viaene, P., Blust, R., Vereecken, H., & De Boeck, G. (2008). A comparison of swimming capacity and energy use in seven European freshwater fish species. *Ecology of Freshwater Fish*, *17*, 284–291.

Wahl, T. (2003). Despiking acoustic Doppler Velocimeter data. *Discussion. Journal of Hydraulic Engineering*, *129*(6), 484–487.

Wang, H., & Chanson, H. (2018). Modelling upstream fish passage in standard box culverts: Interplay between turbulence, fish kinematics and energetics. *River Research and Applications*, *34*(3), 244–252.

Zhang, G., & Chanson, H. (2018). Three-dimensional numerical simulations of smooth, asymmetrically roughened, and baffled culverts for upstream Passage of small-bodied fish. *River Research and Applications*, *34*(8), 957–964.

SUPPORTING INFORMATION

Additional supporting information can be found online in the Supporting Information section at the end of this article.

How to cite this article: Harley, J., Wong, H. L., & Chanson, H. (2024). Anchor chains—A simple low-cost device to assist passage of small-bodied mass fish. *River Research and Applications*, *40*(10), 1954–1970. https://doi.org/10.1002/rra.4347

APPENDIX A

DIGITAL APPENDIX

Visual observations of smooth rectangular channel operations were carried out in the laboratory. The movies showed various dye injections tests conducted in the smooth rectangular channel fitted with a single 13 mm diameter anchor chain.

Table A-1 Video movies of smooth rectangular channel operations.